3D fs-laser nanolithography of YAG crystals: Longitudinal and transversal writing and observation of different phases of crystalline modification

End of Degree Project submitted to

DEPARTMENT OF PHYSICS, University of La Laguna *in partial fulfilment of the requirements for*

Degree in Physics

by

Urma González Tombolato

under the supervision of

Airán Ródenas Seguí

and with assistance of Franzette Paz-Buclatin

DEPARTMENT OF PHYSICS

UNIVERSITY OF LA LAGUNA

San Cristóbal de La Laguna

Santa Cruz de Tenerife, Canarias, España

July 2023

Abstract

Ultrafast laser nanolithography of materials is an area of material development and modification that uses laser pulses with very short durations in order to cause modifications inside a material. It is an important subject of research related to diverse fields, ranging from photonics to microbiology. In this end of degree project, the aim was to study the effect of the variation of a few key parameters in the final outcome of the fabrication of different structures of particular relevance, namely planes, disks and 2D arrays of nanopores. To this purpose, the structures were etched into yttrium-aluminium garnet (YAG) crystals using a combination of femtosecond laser writing and wet etching, and then studied using primarily scanning electron microscopy (SEM). The analysis provided confirmation of known results, as well as new information about the difficulties faced in the fabrication of these structures, such as the appearance of a solid phase within the YAG that was unaffected by the wet-etching for high enough laser power and pulse dose. It also provided examples of both transversal and longitudinal writing, and the differences between them. Finally, in the conclusions section, some possible continuations to these lines of research are proposed.

Resumen

La nanolitografía láser ultrarrápida de materiales es un área de desarrollo y modificación de materiales que utiliza pulsos láser de muy corta duración para provocar modificaciones en el interior de un material. Es un importante tema de investigación relacionado con diversos campos, que van desde la fotónica a la microbiología. En este proyecto fin de carrera, el objetivo era estudiar el efecto de la variación de unos pocos parámetros clave en el resultado final de la fabricación de diferentes estructuras de especial relevancia, a saber, planos, discos y matrices 2D de nanoporos. Para ello, las estructuras se grabaron en cristales de granate de itrio y aluminio (YAG) mediante una combinación de escritura por láser de femtosegundos y ataque químico, y luego se estudiaron utilizando principalmente microscopía electrónica de barrido (SEM). El análisis confirmó resultados ya conocidos y aportó nueva información sobre las dificultades encontradas en la fabricación de estas estructuras, como la aparición de una fase sólida dentro del YAG que no se vio afectada por el ataque químico para potencia del láser y dosis de pulsos suficientemente altas. También se ofrecen ejemplos de escritura transversal y longitudinal, así como las diferencias entre ambas. Finalmente, en el apartado de conclusiones, se proponen algunas posibles continuaciones a estas líneas de investigación.

Contents

Chapter 1

Introduction

En esta introducción se establece la relevancia del tema de estudio, en particular la utilidad de la nanoestructuración en materiales, y de la escritura con láser de femtosegundos en particular, destacando su versatilidad debido a la flexibilidad en los parámetros y aplicabilidad. Es un tipo de escritura particular gracias a la corta duración de los pulsos, que permiten que las interacciones entre los fotones y el material ocurran antes de que haya tiempo para interacciones térmicas, evitando así daños térmicos y permitiendo mayor resolución en las estructuras fabricadas. Asimismo, se presenta una visión general de la motivación detrás de este trabajo de fin de grado, que es estudiar las limitaciones de esta técnica: la resolución espacial posible, los efectos a escalas micrométricas así como milimétricas, y la presencia de estrés y fracturas cuando se deposita energía excesiva en la red cristalina. A este efecto, se estudia el efecto de las distintas combinaciones de parámetros en el resultado de diversas fabricaciones tanto transversales (escritura perpendicular al eje de propagación de los pulsos del láser: planos y discos) como longitudinales (escritura a lo largo del eje de propagación del láser: nanoporos).

In the race for technology development, the production of smaller, more efficient, and cost-effective devices has led to an increase in research into nanostructuring of materials. With its ability to manipulate material properties by use of nanoscale features, it allows for enhancement of material performance, giving them improved mechanical strength and better optical and electrical properties, amongst others, making this a relevant field of research with numerous applications to other subjects such as photonics [1] [2], microelectromechanical systems (MEMS) [3], or biology, where they are used to write structures inside hydrogels used for cell growth [4]. Direct laser writing (DLW), and specifically ultrafast laser inscription of structures offers unique advantages due to its high flexibility in both irradiation parameters and applicability, as well as its cleanliness [5].

Ultrafast laser (also known as femtosecond laser) processing of materials uses laser pulses with durations in the femtosecond range (10^{-15} seconds) focused inside the material (as was the case in this work) or on its surface. Thanks to the short duration of the pulses, the interactions happen before there is time for the material to heat, which prevents excessive thermal damages and allows for higher resolution in the fabricated structures. When they are absorbed, they generate nonlinear processes in the focal volume, such as two-photon or multiphoton absorption, which modify the refractive index of the material. In the present work, we use this method in combination with wet etching, taking advantage of previous studies that have shown a high etching selectivity in similarly irradiated materials [6].

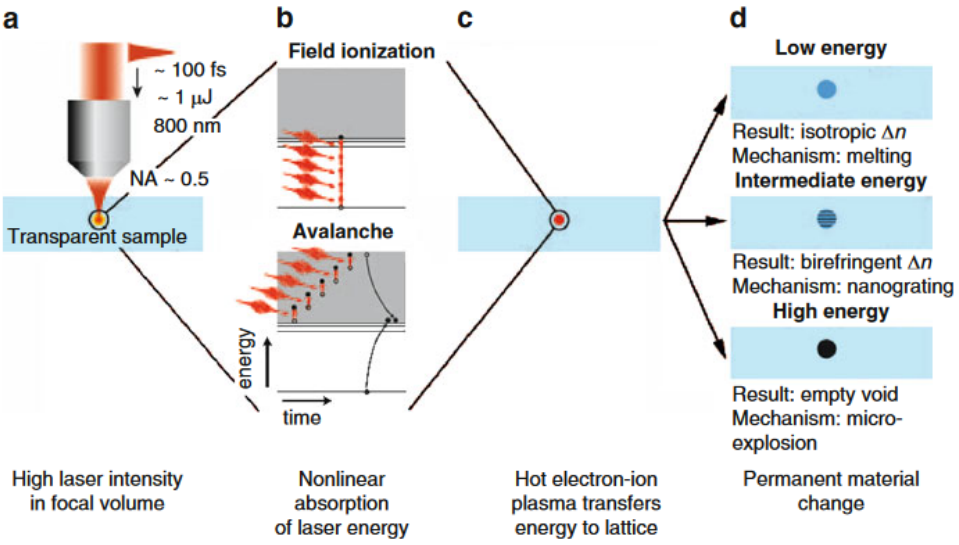

FIGURE 1.1: Scheme of the interaction between femtosecond laser pulses and a material [7]. The laser is first focused in the bulk of the material (a), which causes a nonlinear absorption of its energy by the material (b), creating a hot electron-ion plasma which transfers its energy to the crystal lattice (c) resulting in one of three types of modifications (d).

In Fig. 1.1, a scheme of the physical interaction between the laser and the crystal is shown. Of the three possible modifications, this work focuses only on the low-energy modifications. As the material absorbs the energy from the laser pulse, localized melting causes the lattice structure to be modified in the irradiated areas, which in turn makes the atoms in these areas more susceptible to the reagents present in the wet etching phase. This is what is referred to as higher etching selectivity, and it is dependent on the etchant as well as the material being etched.

The present work aims to approach the identification of optimal etching parameters in simple structures, in order to further pave the ground for future research.

Three structures were etched into YAG crystals: a series of planes, several arrays of disks and a series of arrays of nanopores. Both the planes and disks were fabricated using transversal writing, while the pores were created using longitudinal writing.

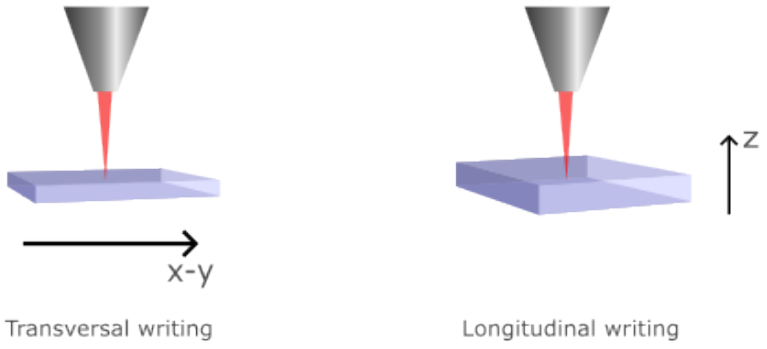

FIGURE 1.2: An illustration of the difference between transversal writing, in which the sample is moved on the plane perpendicular to the propagation axis of the laser pulse; and longitudinal writing, in which the sample moves along the propagation axis.

The planes were chosen as it is one of the simplest shapes to produce: as can be seen Fig. 1.3, the laser writes a series of pores in a row, and the spacing between them determines whether they are separate pores or merge in order to form a plane. This made them a prime candidate for the study of a wide range of manufacturing parameters, in order to find a first approximation to an optimal set of parameters for future fabrications. The disks were an evolution of this concept.

As for the nanopores, they were chosen as they can be used to create photonic crystals, following recent developments in research aimed at manufacturing scintillators.

The main current bottlenecks in this 3D nanolithography technique are:

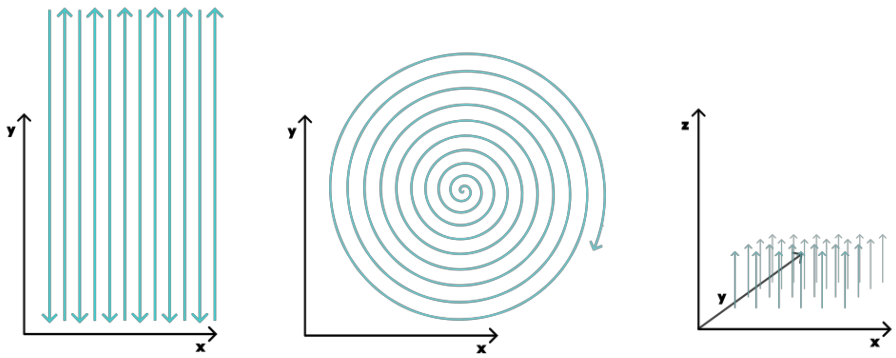

FIGURE 1.3: Scheme of the laser path during etching for the three fabrications.

1. the achievable spatial resolution
2. the footprints in the micron and mm scale
3. stress and cracks that appear when excesive energy is deposited on the crystalline lattice.

This End of Degree Project (TFG) tackles all of these points, with special emphasis put on the identification of detrimental conditions which lead to the undesired cracking at the microscale. The work analyzes which parameters lead to cracks and undesired effects, both in longitudinal and transversal writing, and for geometrically diverse architectures of great technological importance: 2D (horizontal) planes, circular (horizontal) structures, vertical structures. Horizontal here refers to the plane transversal to the writing optical focusing axis, and vertical refers to the axis along the writing focus beam (see Fig. 1.2).

This work also studies the effect of different pulse doses (in pulses/m) and energy doses (in J/m). These can be calculated from the fabrication parameters (mean power, writing speed and frequency) using the following equations:

$$dose = \frac{f\,[kHz] \cdot 10^{3}}{speed\,[mm/s] \cdot 10^{-3}} \tag{1.1}$$

$$E_p\,[nJ] = \frac{P\,[mW] \cdot 10^{6}}{f\,[kHz] \cdot 10^{3}} \tag{1.2}$$

1.1 Objectives

The main goals of this work were:

- Familiarizing oneself with the process of 3D fabrication of nanostructures by means of ultrafast 3D laser nanolithography and wet etching;
- Applying this to the fabrication of different microplanes inside an yttrium-aluminium garnet optical crystals with a wide range of parameters;
- Analyzing by means of microscopy methods the obtained structures in order to determine which parameters are adequate for future reference;
- The creation of more complex patterns (microdisks) using as reference parameters the ones obtained in the previous step;
- The manufacturing of a longitudinally written 2D array of vertical nanopores, as well as their characterization.

1.2 Objetivos

Los principales objetivos de este trabajo son:

- Familiarizarse con el proceso de fabricación 3D de nanoestructuras mediante nanolitografía 3D con láser ultrarrápido y ataque químisco;
- Su aplicación a la fabricación de diferentes microplanos dentro de un cristal óptico de granate de itrio y aluminio con una amplia gama de parámetros;
- Analizar mediante métodos de microscopía las estructuras obtenidas para determinar qué parámetros son adecuados para futura referencia;
- La creación de patrones más complejos (microdiscos) utilizando como parámetros de referencia los obtenidos en el paso anterior;
- La fabricación de una matriz 2D de nanoporos verticales escritos longitudinalmente, así como su caracterización.

Chapter 2

Methodology

En este capítulo se detalla el procedimiento de fabricación de las tres estructuras. En los tres casos se utilizó el mismo láser con la misma configuración del banco óptico, visible en la figura 2.1. La escritura se realizó controlando la potencia del láser con un polarizador y el movimiento de la muestra con una plataforma que podía moverse en las 3 dimensiones espaciales. Tras la escritura láser, la muestra fue pulida para exponer el cristal modificado al ácido utilizado en el ataque químico. Los códigos para las tres fabricaciones se hallan recogidos en el Apéndice A. La primera de ellas fueron una serie de microplanos, planos de aire dentro del cristal, que tenían una longitud de 1 mm pero anchuras del orden de micras, y alturas menores a una micra. Estos planos son la base de la fabricación de estructuras fotónicas en 3D. Pese a que el resultado esperado eran 35 planos con potencias entre 13 y 25 mW y separaciones entre poros de entre 20 nm y una micra, solamente 32 de estos planos fueron escritos. La segunda fabricación fueron unos microdiscos con distinta separación entre anillos consecutivos (100 y 200 nm) y varias potencias (entre 13 y 18 mW). Finalmente, se escribieron unos nanoporos longitudinalmente con el objetivo de crear cristales fotónicos en 2D. De nuevo se exploraron una serie de parámetros, utilizando distintas velocidades de escritura (0,05 y 0,025 mm/s) y potencias.

Three fabrications were made using the following setup:

FIGURE 2.1: Experimental setup for the laser inscriptions. Labeled as 1 is the fs laser used, a Carbide model. The laser light is then redirected to the top of the structure to its right labeled as 2. It is then redirected downwards (3) into a lens (4) on an air suspension chamber, which focuses the light onto the sample affixed to the moving platform below it (5). There is also a camera (6) that allows a real-time vision of the sample, as well as a temperature and humidity control device (7).

The process was as following: first, a YAG crystal was affixed to a microscope slide using a polymer and placed in the mobile holding platform. The desired pattern was programmed into the computer that controlled the platform with the sample on it and some other optical elements (shutter and a polarizer which rotates in order to change the effective power that reaches the sample). After this, the crystal is removed from the slide with acetone and cleaned before beginning the next step.

The irradiated sample is then polished using a mechanical polisher in order to expose the irradiated sections, before placing it in a container with a 35% solution of phosphoric acid in water for the wet etching process, after which it is ready for testing.

2.1 μPlanes

Microplanes are air planes inside the crystals with lateral lengths on the tens or hundreds of microns, and even on the mm scale, since this only depends on the available range of motion of the positioning stages. The μ-planes thickness however is on the sub-micron level.

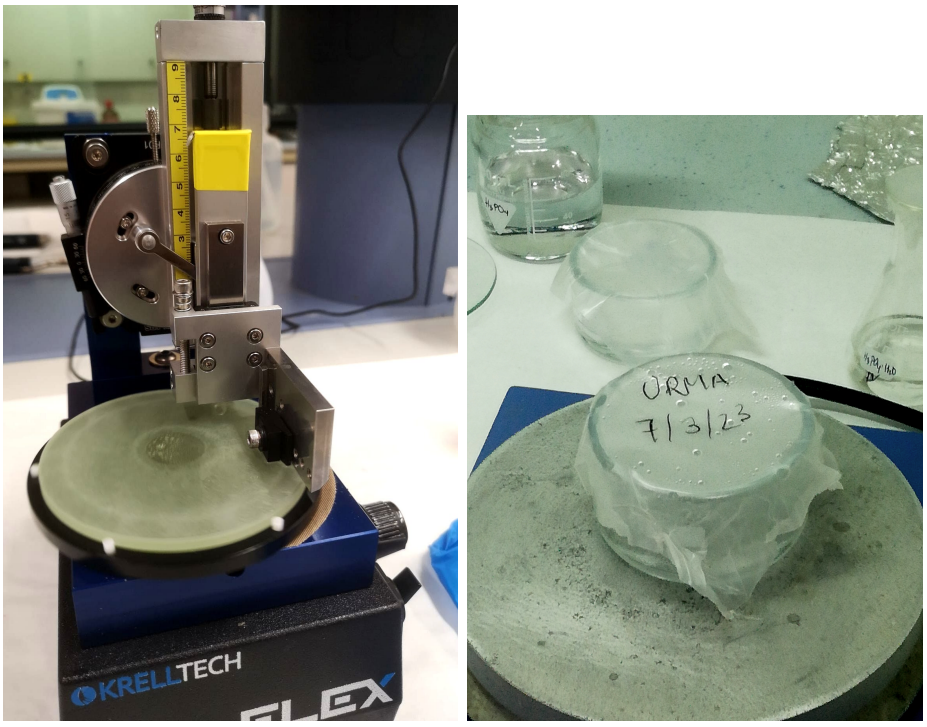

FIGURE 2.2: On the left, a waveguide polisher used in the first and second fabrications. The sample is affixed to the metallic structure parallel to the rotating disk, which has a small rugosity. On the right, the first sample during the wet etching process.

These μ-planes are key for the fabrication of 3D photonic architectures and devices inside optical crystals such as YAG laser crystals. The purpose of this first part of the work is to perform a first rough parameters investigation and evaluate the potential feasibility of these μ-planes.

The first code in Appendix A details the first fabrication. In it, a series of planes with different fabrication parameters (laser power and scan spacing) were implemented, and etched in a YAG sample. The intended result were 35 planes with powers ranging between 13-25 mW and pore lateral scan separations between 20 nm and 1 μm; All planes have a lateral width of 10 μm and a length (along the line scans) of 1 mm.

Upon inspection by optical transmission imaging and by SEM, it was first found that the first two μ-planes had not been etched. The laser was set to 1 MHz and a writing speed of 1 mm s^{-1}. This means that the planes received an initial irradiation dose of 10^9 pulses per meter. Taking the pulse energy into account as given by Eq. 1.2, we get doses between 13 and 25 mJ/mm. This is the pulse dose that affected previously unmodified sections of the crystal as the scan is performed, not counting the further effects of radiation overexposure that happens due to overlapping of laser scans, as the neighboring scan lines are sensitive not only to the writing dose but also the degree of overlapping, as the laser had a focal

spot diameter of $\approx$ 600 nm.
In this section we therefore set a preliminar map of parameters influencing the type of crystalline modifications that are produced as seen from the etching results observed. Effects of laser pulse energy and scan separation are therefore revealed. These can then be extrapolated to other writing geometries, analyzed in the second and third sections (μ-discs and vertical pores).

2.2 μDisks

In a second research phase, μ-discs were fabricated, as they are the base for advanced photonic stuctures such as micro-rings, microlenses, and others key photonic devices with key features on the sub-micron scale. In this case, the writing is not linear anymore as with μ-planes, but circular. This means that similar results are expected in terms of pulse doses and wet etching, but different different cummulative effects and a different response from the crystalline material may be expected.
The second code in Appendix A details the second fabrication. In it, a series of circular disks with different parameters were etched into a YAG sample. The laser was also set to 1 MHz, but the writing speed varied in the sample as a function of the ring radius according to the following equation: $0.00167 + 0.66667 \cdot R$. Two types of disks were etched: one with a ring separation of 100 nm and another with a ring separation of 200 nm. For each ring separation, disks with powers ranging from 13 to 18 mW in increments of 1 mW were etched.

The dose (not accounting for overlapping) is represented in Fig. 2.3. As can be seen in the figure, the dose decreases as the ring radius increases. Taking the pulse energy into account, we get that the disks were written with doses between 2.5 and 7.5 J/mm.

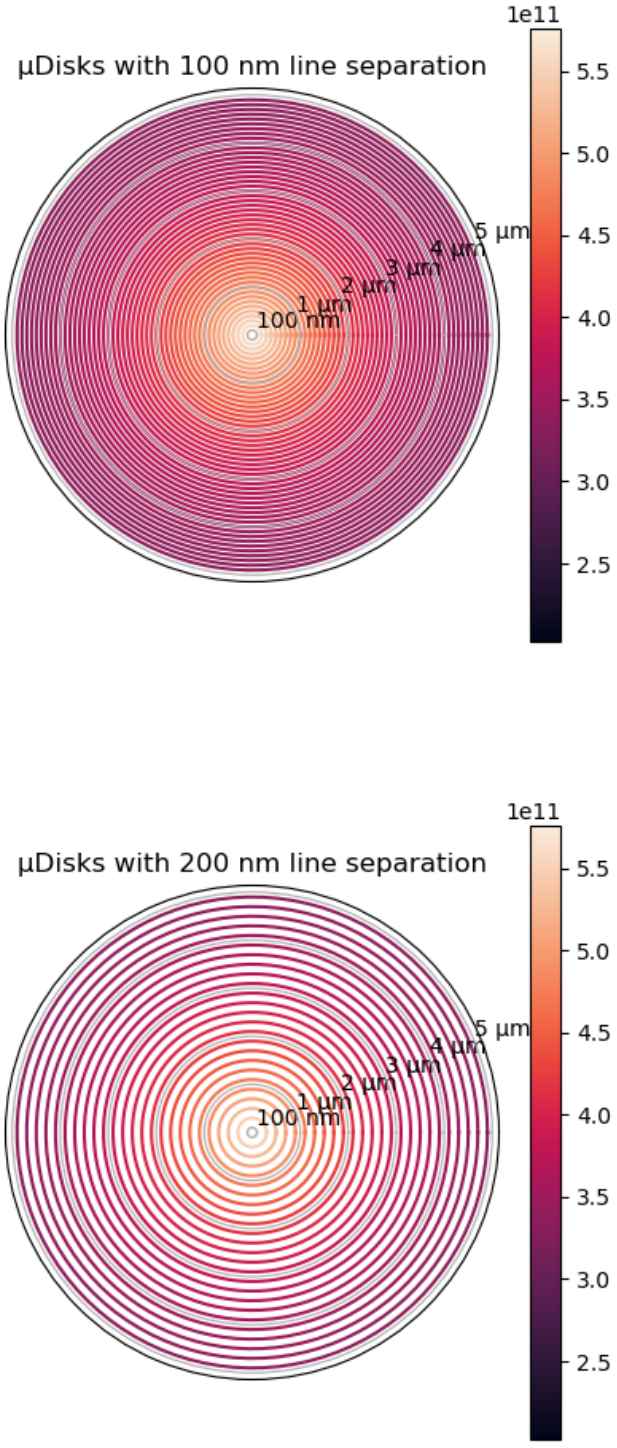

FIGURE 2.3: Dose of radiation in the microdisks for the two different ring separations, as a function of the ring radius.

2.3 nPores

Finally, a different writing scheme was explored which is vertical writing, where the line scans are performed along the optical axis rather than transversely as in the previous sections. The aim here is to fabricated 2D photonic crystals lattices with feature sizes on the sub-micron scale and lattice spacings on the micron level.
The third code in Appendix A details the last fabrication. In it, a series of longitudinal pores with different powers were etched into a YAG sample. The laser was also set to 1 MHz, but two different writing speeds were used: 0.05 mm/s and 0.025 mm/s; for a dose of either $2 \cdot 10^{10}$ or $4 \cdot 10^{10}$ pulses/m, and powers comprised between 12 and 14 mW. This means the energy doses were between 250 and 560 mJ/mm.

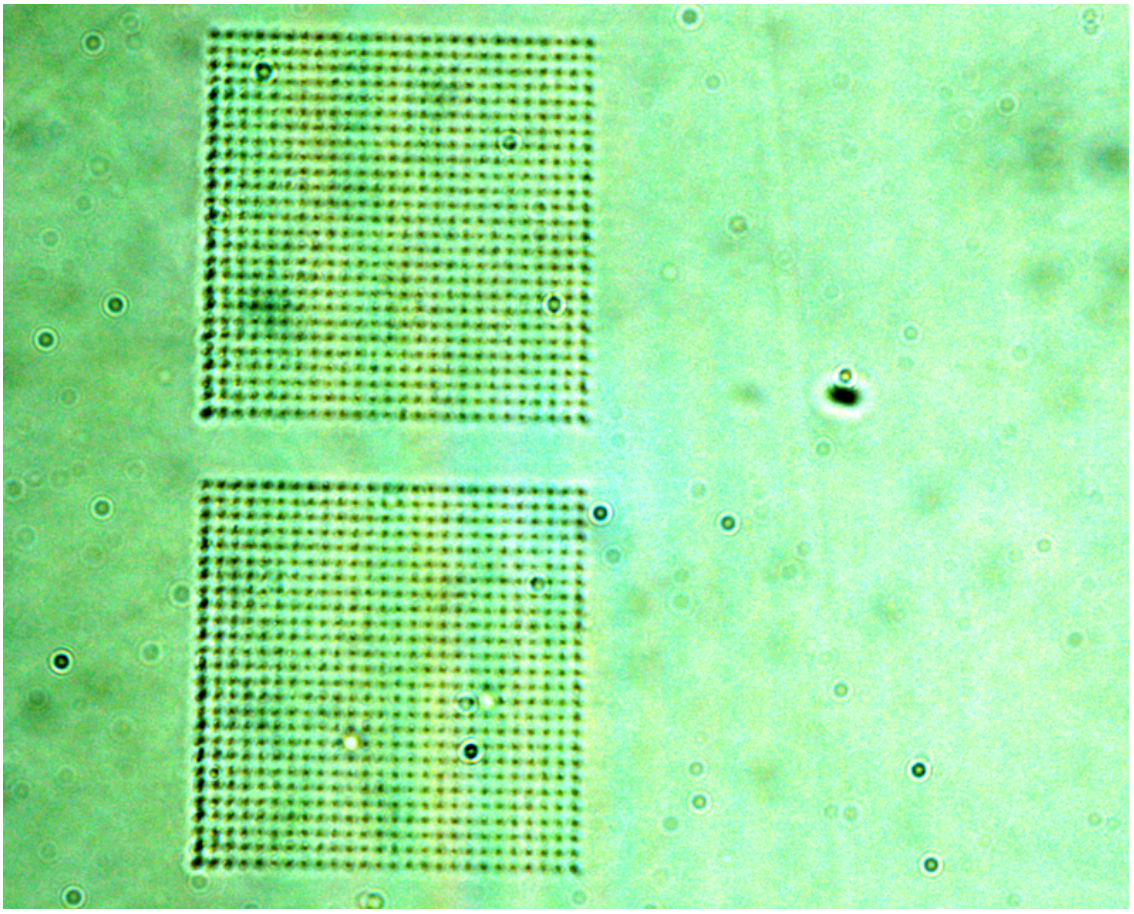

FIGURE 2.4: Optical image of two square-lattice 2D arrays of nanopores. Lattice spacing was chosen to 2 μm so as to evaluate easily individual nanopores. Typical pore widths were observed to be on the 200 nm down to 100 nm

Chapter 3

Results and Discussion

Aquí se presentan los resultados obtenidos. Para los planos: se realizaron medidas de los poros separados para analizar efectos de proximidad, sin resultados concluyentes, y de las alturas de los planos, observándose que aumenta con la potencia. También se realizó un estudio cualitativo de la calidad de los planos obtenidos, teniendo en cuenta la cantidad de cracks así como la presencia o ausencia de material residual dentro de los mismos, y se establece una relación entre este estudio y resultados obtenidos por F. Paz-Buclatin y A. Ródenas presentados en la figura 3.6. Para los discos: se observaron dificultades en el posicionamiento vertical del foco del láser debido a variaciones en la temperatura del laboratorio, que se tradujeron en variaciones en la posición vertical de la muestra. Asimismo, se relaciona la dosis preliminar de pulsos con la presencia de material dentro de los discos tras ataque químico, de forma similar a algunos de los planos. Para los poros: se observó una circularidad excepcional en la escritura vertical, especialmente comparando estos poros con los presentados en el apartado de los planos. También se señala el buen resultado del ataque químico.

3.1 μPlanes

The first two planes (in black in the figure 3.1) were not etched into the crystal as the laser did not have enough power to cause a modification in the material that resulted in a significant difference in etching selectivity. Interestingly, the next planes for the same laser power but less pore separation did show in SEM imaging, this meaning that the accumulation of irradiation in the same area was enough to cause modifications in the material regardless of the low laser power. This points to the presence of incubation effects, something not observed before for this type of experiments. The rest of the planes etched with the same power present significant cracking that is particularly severe in

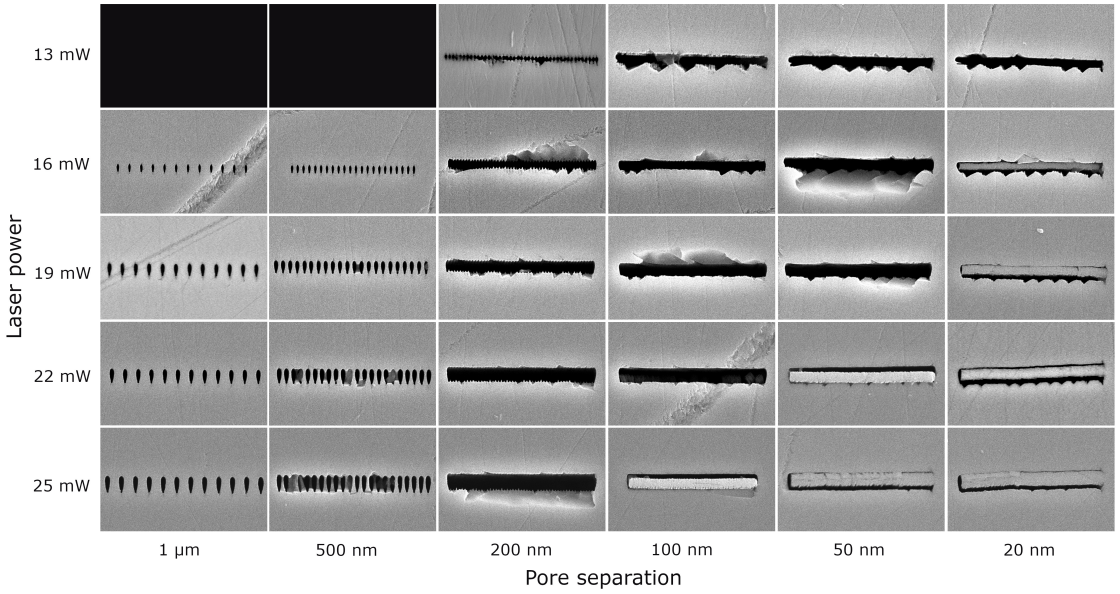

FIGURE 3.1: SEM images for the etched planes, showing the results of the different combinations of power and scan spacing.

the bottom side (which happened to be the side farthest from the crystal surface), as the stress accumulated within the material due to the cumulative dose of irradiation is received. It is important to note that these cracks result from the mechanical polishing of the material. If no cracks are observed then we conclude that the fabrication conditions are good since polishing does not entail cracking. However, minor cracks do always appear in the processing window here studied, fixed to a 1 MHz pulse repetition rate and 1 mm/s speeds. Many more experiments can be done beyond these parameters, in possible future works.

The pore widths and heights were also measured for the first two scan spacings as they had separated pores, in order to determine if there was any proximity effect, i.e. a change in apparent pore cross-sectional sizes due to proximity effects. The results are plotted in Fig. 3.2, and it shows that for low laser power the size of the pores was very similar independently of the pore separation, but for higher powers the pore width is measured to be slightly smaller for the lower pore separation. We interpret these results in terms of stress accumulation effects. Each laser line scan produces a longitudinal track with possibly compressive stress on its sides. This stress has a maximum at the pore boundary and extends outwards. When two neightbouring tracks are written their overlapping effects may modify their final lattice stress profiles, this possibly affecting the final pore widths the higher the pulse energy (i.e. laser power) and the lower the scan separation. So, preliminary findings are also obtained in this section, that proximity effects may do exist.

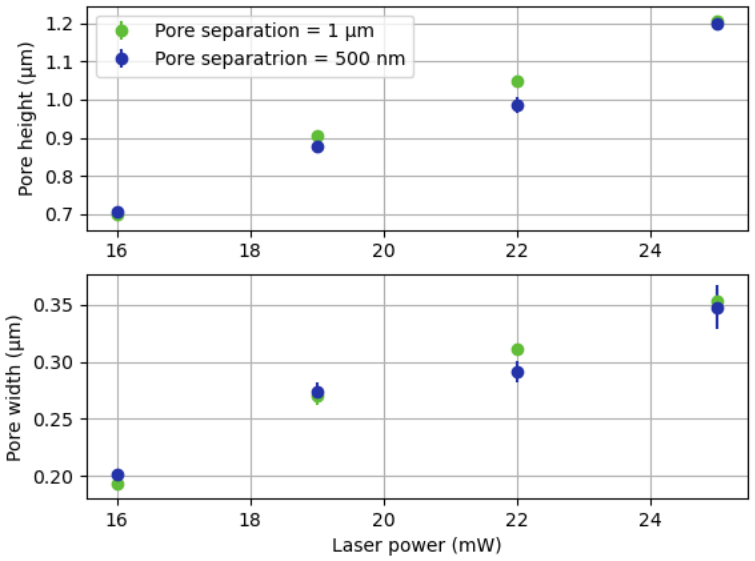

FIGURE 3.2: Measurements of the pore width and height for different energies and pore separations.

Further experiments with much more detailed parameters are certainly needed to assess this effects.

For every power, the scan spacings of 1 μm and 500 nm were comprised of separate, defined pores, and only from the third scan spacing of 200 nm and lower values, there were proper fully homogeneous planes. Planes written at given scan separations show a behaviour consisting on more cracks for the lower pulse energies, less cracks for medium pulse energies, and remnant material for the highest powers. This behaviour indicates the presence of different phases of material photo-modification, which is revealed here from their different chemical wet-etching behaviours. This is expected since chemical wet-etching is highly sensitive to lattice strain and molecular orientations, so the larger the distortion of the lattice (due to stress) the higher the wet-etching rate.

However, as mentioned, some of the planes had material left inside even after undergoing polishing and wet etching, indicating the possibility of the high dose of irradiation received (note the gradient of planes with crystal left inside, forming a quasi-triangular shape for the combinations of least space between pores and most laser power) being responsible for the creation of a new crystalline phase inside the planes. The boundary region between the original un-etched YAG structure and the photo-modified one does etch, but material inside is observed un-etched, therefore a new phase has been here discovered for nanolithography of YAG crystals.

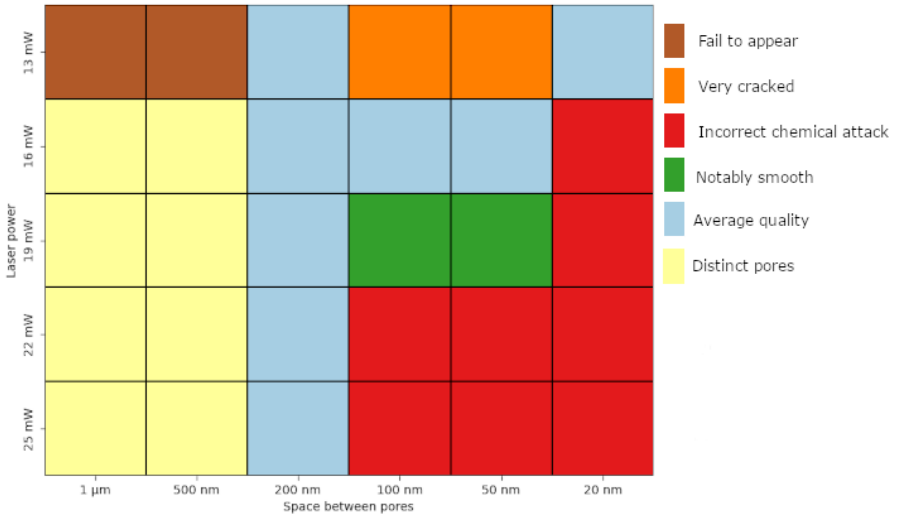

FIGURE 3.3: Classification of the aforementioned planes for future reference. In brown, the combinations of power and scan spacing that did not show. In yellow, combinations that resulted in separated pores with no overlapping. In orange, planes that were very cracked as a result of excess stress in the material induced by the laser. In red, planes that presented residual material inside them. In green, planes that were very smooth, indicating good parameters for future fabrications.

The plane heights were measured using the digital image processing software ImageJ, of which a screenshot is shown in Fig. 3.4. As cracking was present, five measurements for the width of each plane were taken in different places, avoiding the cracked parts as much as it was possible, and then averaged. The results are shown in Fig. 3.5. Results show that indeed the pulse energy allows to control the plane vertical width with a certain independence from the scan spacing. Between 100 nm and 200 nm the best scan separation is obtained for the general conditions here studied.

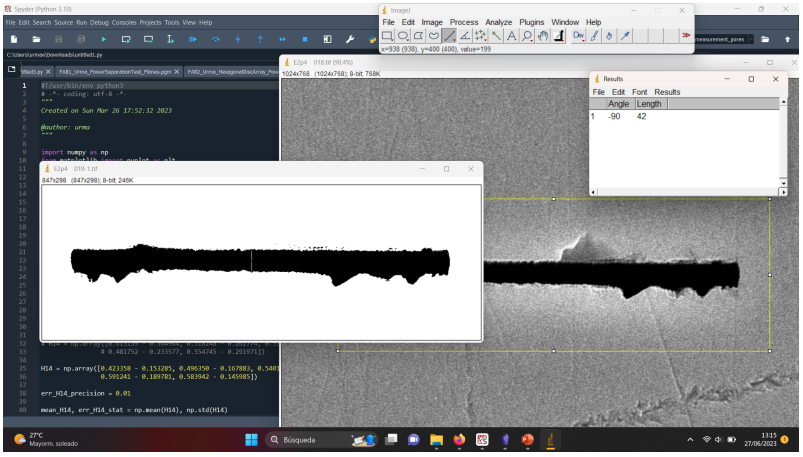

FIGURE 3.4: Screenshot of the measuring process using the image processing software ImageJ.

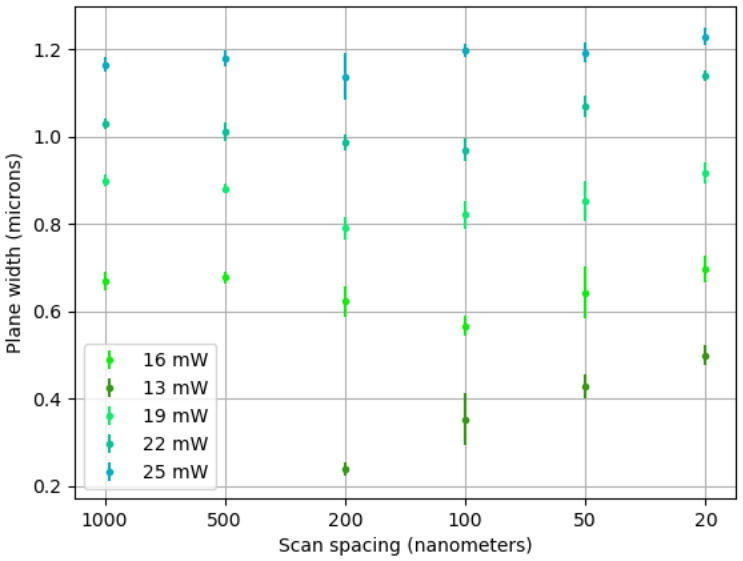

FIGURE 3.5: Measured width of the microplanes for different scan spacings and powers. The first two measurements for each power are the separate pores, while the rest are for the planes proper.

According to recent research of the research group (LeapLab group of the Physics Department, ULL) (see Fig. 3.6), the following pattern has been found for the rate of chemical wet-etching rate in relation to the dose of irradiation used. For very low doses of pulse irradiation ("low dose" in the graph), no chemical wet-etching is achieved as the material does not undergo significant enough modifications. On the zone labeled as "linear", the etch rate grows linearly with dose as stress increases. On the zone labeled as "plateau", the etch rate hits a halt and stays constant. This is possibly related to material reaching the maximal stress sustainable before bond breaking (related to its Young modulus) and the creation of nanocracks that relax the stress in the material, which would correspond to the more cracked planes in Figure 3.1. This plateau zone would therefore coincide with maximal stress and therefore although single pores etch very fast, it should be avoided when writing in a multiscan approach.

On the zone labeled as "decrease", the etching rate drops exponentially to a residual level as nanocracks form in the material before etching, relaxing stress. Finally, a new zone not depicted in the diagram is reached for even higher doses, in which the material inside the plane reaches a different stable phase, which results in a successful chemical attack only in the external boundary between the unmodified crystal and the new phase, and this volume stays unetched. Further investigations of this sub-micron regions is needed to understand

its composition and/or lattice structure.

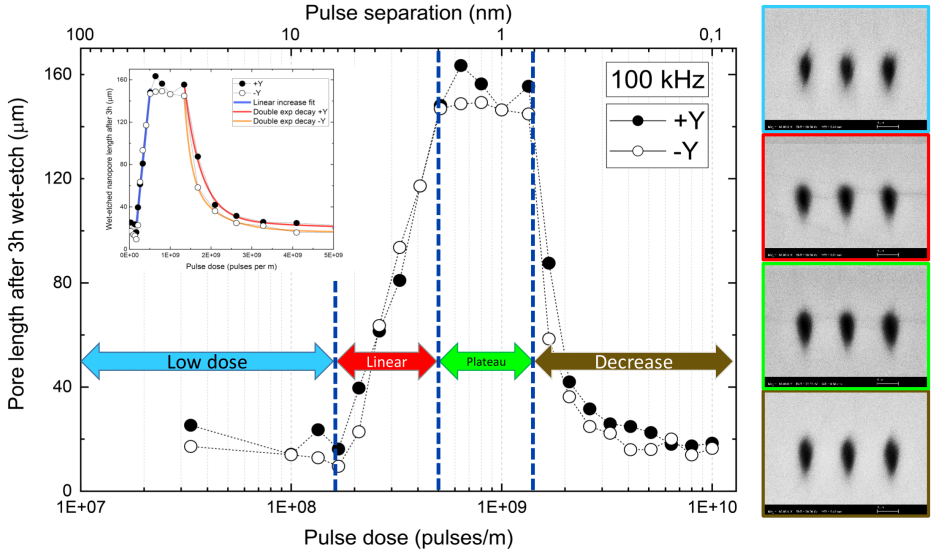

FIGURE 3.6: Etching rate vs pulse dose in logarithmic scale. Four regions can be seen, each with a SEM image of pores made with a dose corresponding to one of the four regimes. These experiments were done at 100 kHz pulse rep. rate with pulse energies of 19 nJ, circular pol., and varying scan speeds. Unpublished results from F. Paz-Buclatin and A. Ródenas, 2023

3.2 μDisks

FIGURE 3.7: Optical imaging of some of the microdisks. On the left, disks that were written at different heights. Note how some (leftmost column and rightmost column, though this one slightly less) appear out of focus. On the right, disks that are at the same depth.

After the etching of the microdisks, optical imaging (as seen in Fig. 3.7) revealed that not all disks were written at the same depth (see Fig. 3.8), as focusing on some of them made the others appear out of focus. This was later confirmed by SEM imaging, done after polishing of the sample and chemical attack, shown in Fig. 3.8. This variation in the depth of the disks is likely due to variations in the temperature of the room in which the etching was done, which caused the platform which held the sample to move.

It is also noteworthy that the disks had material left inside them in a similar fashion as the planes depicted in red in Fig. 3.3. Considering the pulse dose, even without considering overwriting, we can see it's beyond the limit on Fig. 3.6, which is consistent with the aforementioned new regime beyond the limits on the x axis in the figure.

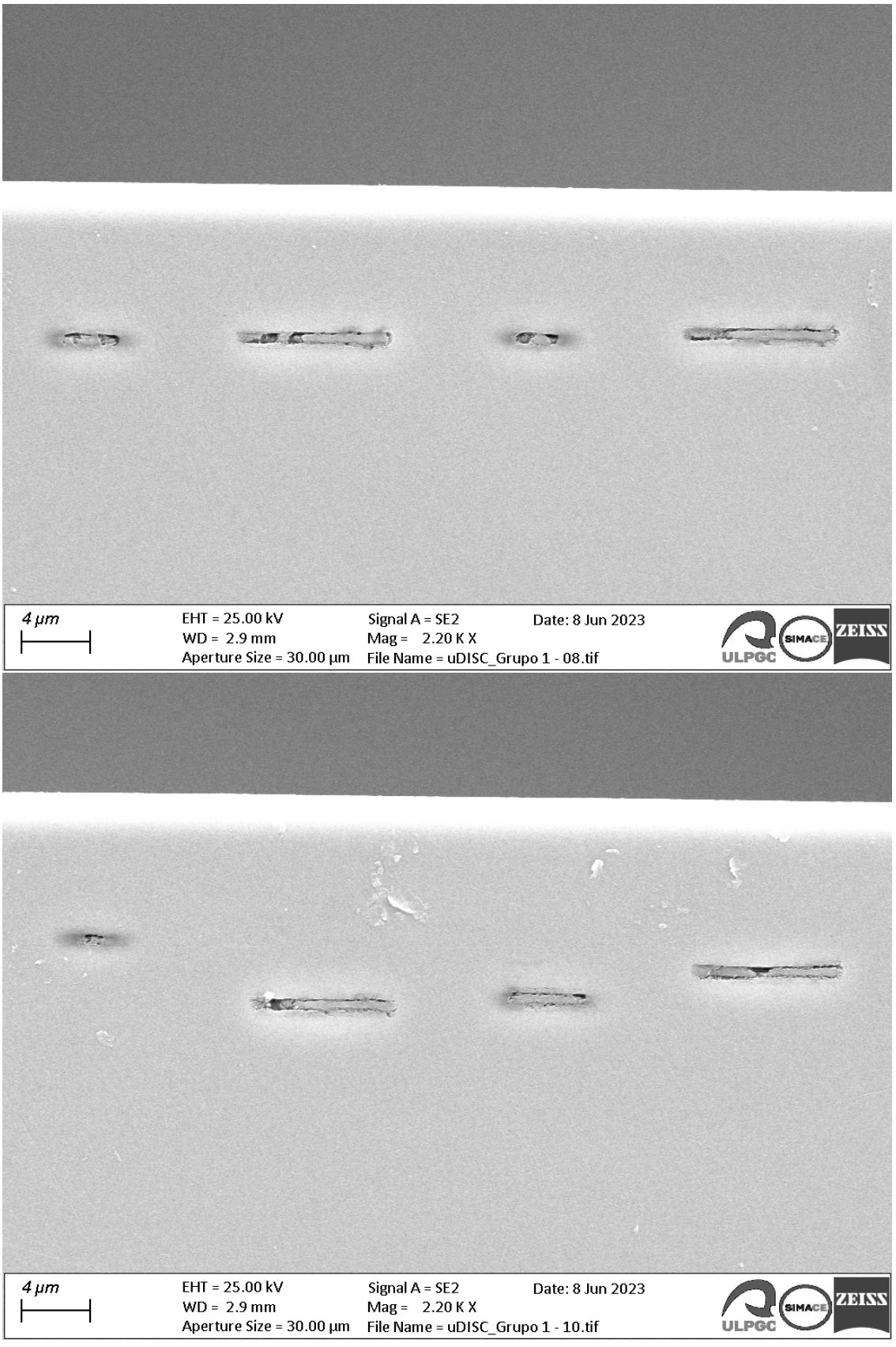

FIGURE 3.8: SEM imaging of some of the microdisks. As it can be seen, they are near the surface of the sample crystal. The varying sizes of the visible profiles are due to the fact that the polishing cut disks from different arrays at different distances from the center of the disks.

3.3 nPores

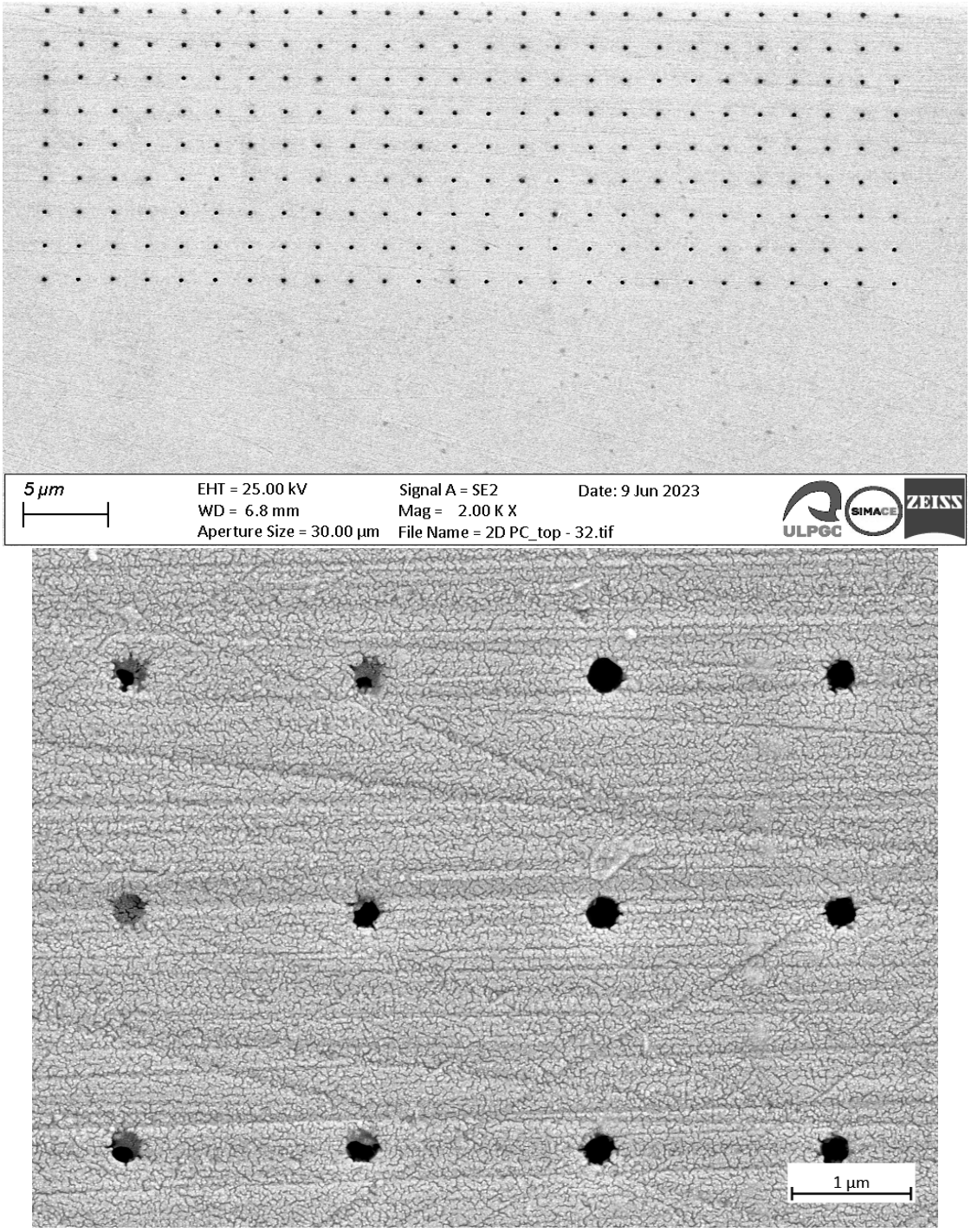

FIGURE 3.9: On the top, SEM image of part of the square-array nanopores, taken from the top. On the bottom, close-up of the pores on surface.

The pores SEM images were analyzed using ImageJ free software. Each group of 12 pores was fitted to a series of circles, and the diameters of those circles were averaged to obtain

the results displayed in Fig. 3.10. The idea here is to see the pore diameters, at the surface cut across the vertical pores, as a function of power at the point of the longitudinal scan and for the given vertical scan speed.
The results were fitted into lines using a least squares approximation of the form $D = a \cdot P + b$, with the following coefficients:

Speed	a	b
0.05 mm/s	0.035 ± 0.017	-0.2 ± 0.2
0.025 mm/s	0.017 ± 0.005	-0.02 ± 0.07

Both are lines with a positive slope, meaning that the diameter of the pores increases with power as should be expected. All nanopores were successfully etched, and this approach seems highly successful. It is interesting to note the fact that the pores had a higher pulse dose than some of the planes that did un

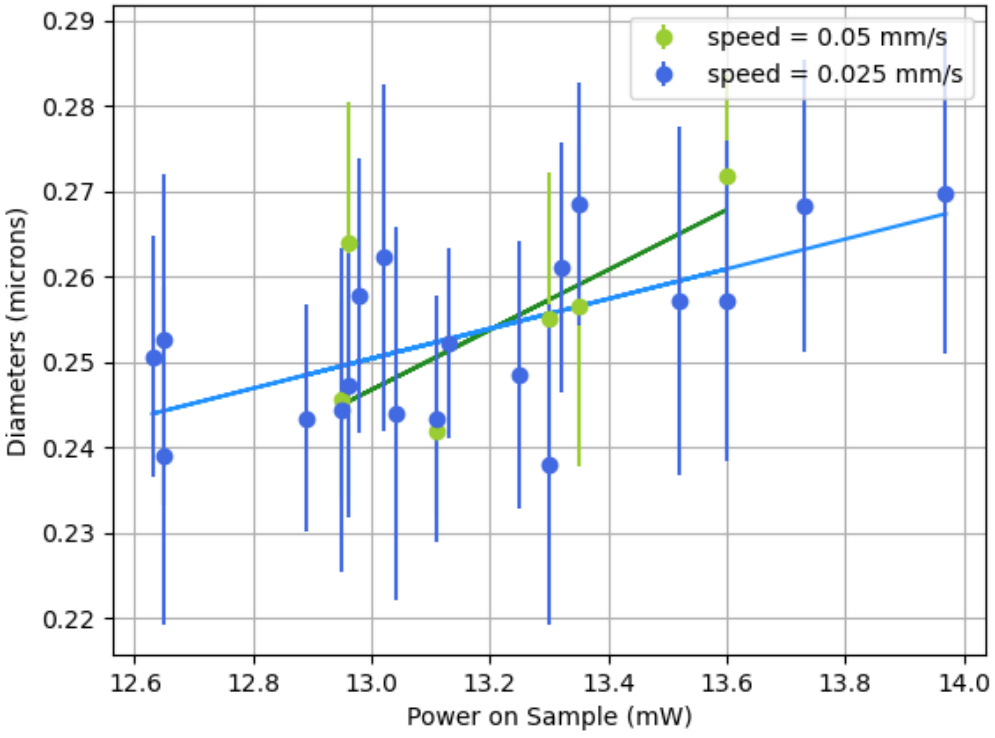

FIGURE 3.10: Measurement of the diameters of the nanopores vs the power with which they were written at that given cross-section depth within the sample, for both 50 and 25 μm/s speeds.

Chapter 4

Conclusion and Future Works

En este último capítulo se resumen las conclusiones a las que se ha llegado. Primeramente, el cumplimiento de los objetivos propuestos al principio de este trabajo con respecto a una primera aproximación al estudio de los parámetros de fabricación y los efectos que surgen en respuesta a distintas configuraciones de los mismos. Se destaca aquí la aparición de una nueva fase de modificación para dosis de pulsos y energía mayores de lo investigado hasta este momento en la que el ataque químico deja de ocurrir. Esto se repitió para los microdiscos, que también presentaron el mismo efecto. También se destaca que este trabajo estudia *grosso modo* los parámetros mencionados, y que es necesario seguir investigando para refinar la optimización de los mismos.

The initial objective behind the fabrication of the planes was to use a simple shape as a basis for studying a wide range of manufacturing parameters, with the aim of optimising said parameters for future work. The result of this test is illustrated in Fig. 3.1, where it can be seen that the planes with pore separation of 100 - 200 nm etched at 22 mW are particularly smooth. Despite the plane corresponding to 100 nm having some residual material inside, this is only a broad first approach, and the next step would be to fine-tune the parameters by realizing more tests, possibly starting at 100 nm and 22 mW and then variating the power in small increments around that value in order to optimize it.

This fabrication also resulted in an interesting finding, namely the presence of planes that had material inside them that was not affected by the etching process, which is hypothesized as a possible different phase of the YAG crystal. This happens for higher doses of pulses and energy than had previously been studied. This can be used as a basis for expanding the results comprised in Fig. 3.6 in future works. Proximity effects and

incubation effects (related to this new phase) were also observed. It is interesting to note that the new phase does not appear in planes that did not have multiscans.

As for the microdisks, the fabrication conditions were not optimal, and temperature fluctuations resulted in the disks not being at the same depth. They also presented residual material inside them, in a similar fashion as the aforementioned planes.

The nanopores were a test for longitudinal writing. Fig. 3.6 again shows the appearance of pores written transversally (note the higher aspect ratio respective to the pores shown in 3.9). A linear relationship between laser power and pore diameter is found to exist. This fabrication, despite having a higher initial dose than the planes, did not present the new modification phase. This is possibly related to the fact that there was no overlapping between the pores. An interesting future experiment would be to make the planes vertically, doing the multiscan longitudinally instead of in the focal plane, and comparing the results of that fabrication to those found here.

Appendix A

Codes

A.1 Planes

```
#define ShutterClose $DO0.Z = 0
#define ShutterOpen $DO0.Z = 1

DVAR $FSHIFT $OFSET $PlaneLength $PlaneWidth $SPEED $AY $DEPTH $LDEPTH $ANGLE
$PWR $PWR_0 $PWR_Delta $ANGLE_0 $Pmax
DVAR $Pmin $Pstep $LossFactor $PWR_Before $SPEEDpos $ind $PoreSep[6] $NumScans
$PlaneSep



' comment
;
// Power Test and Pore Separation Test for Planes

enable X Y Z A
ShutterClose

$FSHIFT = 1.3 'needs recalibration
$OFSET = 0 'needs calibration

$PlaneLength = 1 'Length of the plane (in mm)
$PlaneWidth = 0.010 'Width of the plane (in mm)
$PlaneSep = 0.010  'Separation between planes (in mm)
$SPEED = 1 'writing speed (in mm/s)
```

```
$SPEEDpos = 0.01 'positioning speed (in mm/s)

$LossFactor = 4.4 'Loss factor of laser power from before the expander to the
                sample

//////////////'LASER POWER RANGES that reaches the sample////////////
$Pmax = 25 'Maximum desired power mW
$Pmin = 13 'Minimum desired power in mW
$Pstep = +3 'Power step in mW

////////////'PORE SEPARATION LIST (in mm)///////////////
$PoreSep[0] = 0.001
$PoreSep[1] = 0.0005
$PoreSep[2] = 0.0002
$PoreSep[3] = 0.0001
$PoreSep[4] = 0.00005
$PoreSep[5] = 0.00002

////////////////////////////////////////////////////////////////////
////////////////////////////////////////////////////////////////////

$DEPTH = 0.020   'depth of structure from the surface (in mm)
$LDEPTH = ($DEPTH-$OFSET)/$FSHIFT 'Linear movement of the objective such that
                                the focus is in $DEPTH


////////  PARAMETERS TO CALCULATE THE ANGLE FROM THE DESIRED POWER/////////
////////  TO CALIBRATE THE ANGLE DO FIRST A HARD HOME
  (HOME BUTTON NEXT TO "A" AXIS). ANGLE SHOULD GO TO 0.00º.
////////  THEN MANUALLY INTRODUCE around 47º TO GO CLOSE TO MINIMUM.
  THEN FINE TUNE MINIMUM.

$PWR_0 = 7.22 'Minimum Power in mW
$PWR_Delta = 138.7-$PWR_0 'Max Power - Min Power in mW
$ANGLE_0 = 47.11 'Angle shift in degrees (angle where minimum is located)

////////////////////////////////////////////////////////

G92 X0 Y0 Z0 'set surface Z=0 starting point as coordinate origin
DWELL 1
```

```
VELOCITY ON 'don't decelerate between moves

Linear Z -$LDEPTH F 1 'goes to starting depth
DWELL 1
////////////////////////////////////////////////////////////////
ABSOLUTE

FOR $PWR = $Pmin TO $Pmax STEP $Pstep 'repeat every power step

    ABSOLUTE
    $PWR_Before = $PWR*$LossFactor 'calculate the power needed before the beam
 expander
    CALL GetAngle k($PWR_Before) 'Calculates the corresponding angle for the
 desired power before beam expander
    Linear A $ANGLE F 1 'the power is changed to the new given value

////////////////////////////////////////////////////////////////////////////
    FOR $ind = 0 TO 5 STEP +1
        $NumScans = CEIL($PlaneWidth/(2*$PoreSep[$ind])+1) 'number of times to repeat
  zigzag movement

        REPEAT $NumScans

            INCREMENTAL
            ShutterOpen
            Linear X +$PlaneLength F $SPEED 'writes horizontally
            '(sample moves towards left)
            ShutterClose
            Dwell 0.2

            Linear Y +$PoreSep[$ind] F $SPEEDpos
            'move to another spot vertically upwards
            Dwell 0.1

            ShutterOpen
            Linear X -$PlaneLength F $SPEED
            'writes horizontally (sample moves towards right)
            ShutterClose
            Dwell 0.2

            Linear Y +$PoreSep[$ind] F $SPEEDpos
```

```
            'move to another spot vertically upwards

        ENDREPEAT

        Linear Y +($PlaneSep-$PoreSep[$ind]) F $SPEEDpos 'move to starting point of
  next plane
        DWELL 0.2
    NEXT $ind

////////////////////////////////////////////////////////////////////

NEXT $PWR 'ends the power cycling


////////////////////////////////////////////////////////////////////////////
ShutterClose
END PROGRAM


DFS GetAngle
$ANGLE = ASIN(SQRT(($k - $PWR_0)/$PWR_Delta)) * 180/(2 * Math.PI) + $ANGLE_0
 'PWR must be in mW
ENDDFS
```

A.2 Disks

```
#define ShutterClose $DO0.Z = 0
#define ShutterOpen $DO0.Z = 1

DVAR $FSHIFT $OFSET $Row $Col $Radius $RadiusMin $RadiusMax $RingSeparation
    $YSeparation $XSeparation $XSetSeparation
DVAR $SPEED $SPEEDpos1 $SPEEDpos2 $DEPTH $LDEPTH $ANGLE $PWR
    $PWR_0 $PWR_Delta $ANGLE_0 $Pmax $Pmin $Pstep $LossFactor $PWR_Before

MSGCLEAR 1
MSGCLEAR 2
MSGCLEAR 3
' comment
;
```

```
// Power and Frequency Test for Discs in 8x4 Hexagonal Array

enable X Y Z A
ShutterClose

$FSHIFT = 1.357 'Normally is 1.39 for satsuma IFN setup, needs recalibration
$OFSET = -0.00139  'needs calibration

$Row = 8
$Col = 4 'should be even number
$RadiusMin = 0.0001
$RadiusMax = 0.005
$RingSeparation = 0.0001
$YSeparation = 0.015
$XSeparation = 0.01299
$XSetSeparation = 0.060

$SPEEDpos1 = 0.005 'positioning speed for small distances (in mm/s)
$SPEEDpos2 = 0.05  'positioning speed for large distances

$LossFactor = 4.4 'Loss factor of laser power from before the expander to the sample

//////////////'LASER POWER RANGES that reaches the sample//////////////
$Pmax = 18 'Maximum desired power mW
$Pmin = 11 'Minimum desired power in mW
$Pstep = 1 'Power step in mW

////////////////////////////////////////////////////////////////////////
////////////////////////////////////////////////////////////////////////

$DEPTH = 0.024   'depth of structure from the surface (in mm)
$LDEPTH = ($DEPTH-$OFSET)/$FSHIFT 'Linear movement of the objective such that the
                            'focus is in $DEPTH


////////  PARAMETERS TO CALCULATE THE ANGLE FROM THE DESIRED POWER//////////
////////  TO CALIBRATE THE ANGLE DO FIRST A HARD HOME (HOME BUTTON NEXT TO "A" AXIS.
////////  ANGLE SHOULD GO TO 0.00º.
////////  THEN MANUALLY INTRODUCE around 47º TO GO CLOSE TO MINIMUM.
//////// THEN FINE TUNE MINIMUM).
```

```
$PWR_0 = 0.15 'Minimum Power in mW
$PWR_Delta = 525-$PWR_0 'Max Power - Min Power in mW
$ANGLE_0 = 41.15 'Angle shift in degrees (angle where minimum is located)

////////////////////////////////////////////////////////////////////

G92 X0 Y0 Z0 'set surface Z=0 starting point as coordinate origin
DWELL 1

VELOCITY ON 'don't decelerate between moves

Linear Z -$LDEPTH F 1 'goes to starting depth
DWELL 1
////////////////////////////////////////////////////////////////////

ABSOLUTE

Linear X $RadiusMin F $SPEEDpos1 'Go to starting point

FOR $PWR = $Pmin TO $Pmax STEP $Pstep 'repeat every power step
    MSGDISPLAY 1, "Doing power:", $PWR
    ABSOLUTE
    $PWR_Before = $PWR*$LossFactor 'calculate the power needed
    'before the beam expander
    CALL GetAngle k($PWR_Before) 'Calculates the corresponding angle for the
    ' desired power before beam expander
    Linear A $ANGLE F 1 'the power is changed to the new given value

////////////////////////////////////////////////////////////////////////////
    REPEAT $Col/2
        REPEAT $Row
            FOR $Radius = $RadiusMin TO $RadiusMax STEP $RingSeparation
                INCREMENTAL
                CALL GetSpeed f($Radius)
                ShutterOpen
                CW X0 Y0 I-$Radius J0 F$SPEED
                Linear X +$RingSeparation F $SPEEDpos1
            NEXT $Radius
            ShutterClose
            LINEAR X -$RadiusMax Y +$YSeparation F $SPEEDpos2
        ENDREPEAT
```

```
        MSGDISPLAY 2, "Done col 1"
        LINEAR X +$XSeparation Y -$YSeparation/2

        REPEAT $Row
            FOR $Radius = $RadiusMin TO $RadiusMax STEP $RingSeparation
                INCREMENTAL
                CALL GetSpeed f($Radius)
                ShutterOpen
                CW X0 Y0 I-$Radius J0 F$SPEED
                Linear X +$RingSeparation F $SPEEDpos1
            NEXT $Radius
            ShutterClose
            LINEAR X -$RadiusMax Y -$YSeparation F $SPEEDpos2
        ENDREPEAT
        MSGDISPLAY 2, "Done col 2"
        LINEAR X +$XSeparation Y +$YSeparation/2 F $SPEEDpos2
    ENDREPEAT
    LINEAR X ($XSetSeparation-$XSeparation) F $SPEEDpos2

////////////////////////////////////////////////////////////////////

NEXT $PWR 'ends the power cycling
////////////////////////////////////////////////////////////////////////////
ShutterClose
END PROGRAM


DFS GetAngle
    $ANGLE = ASIN(SQRT(($k - $PWR_0)/$PWR_Delta)) * 180/(2 * Math.PI) + $ANGLE_0
    'PWR must be in mW
ENDDFS

DFS GetSpeed
$SPEED = 0.00167 + 0.66667*$f
ENDDFS
```

A.3 Pores

```
#define ShutterClose $DO0.Z = 0
#define ShutterOpen $DO0.Z = 1
```

```
DVAR $FSHIFT $OFFSET $ARRAY_SIZE $PORE_SEP $ARRAY_SEP $DEPTH_INI $DEG_INI
DVAR $DEPTH_FIN $UniR $RATIO $SPEED $SPEED_array $SPEED_pore $N_PORE $N_ZIGZAG
DVAR $LDEPTH_INI $LDEPTH_FIN $IND1 $IND2 $DEG_30 $SLOPE  $PBUBBLE

$FSHIFT = 1.357
$OFFSET = -0.00139

$ARRAY_SIZE = 0.050 'width and length of one 2D array
$PORE_SEP = 0.002 'vertical pore separation
$ARRAY_SEP = 0.010

////////////////////////////////////////////////////////////////
$DEPTH_INI = 0.040 'bottom depth
$DEPTH_FIN = 0.003 'top sub-surface depth CHEQUEAR!!!!!
////////////////////////////////////////////////////////////////
////////////////////////////////////////////////////////////////
$DEG_30 = 54.4 'angle for 30 um (parameter to be modified each run)
                        ' 24mW (each 0.1deg is 0.3mW)
//////////////////////////////// from 24mW  to 40mW
$PBUBBLE = 50.0    'USUALLY 49.2DEG / FOR 19mW AT 10UM IT WAS 52.29DEG
                         '(ESTO HACE BURBUJA)



$SPEED = 0.025 'vertical writing speed 50 um/s
$SPEED_pore = 0.010 'positioning speed between pores 10 um/s
$SPEED_array = 0.100 'positioning speed between array 100 um/s

$N_PORE = $ARRAY_SIZE/$PORE_SEP+1
$N_ZIGZAG = $N_PORE/2  'number of times zigzag movement is repeated
                        '(n_pore should be even number)
$LDEPTH_INI = ($DEPTH_INI-$OFFSET)/$FSHIFT '0.03050
$LDEPTH_FIN = ($DEPTH_FIN-$OFFSET)/$FSHIFT '0.00323

$SLOPE = ($DEG_30-$PBUBBLE)/(-0.01987)
'power slope from 40 um to 3 um / 49.20deg is Pbubbles
$DEG_INI = $SLOPE*-$LDEPTH_INI+$SLOPE*0.0231+$DEG_30
'required angle for writing in initial depth

$UniR = 0.00784 'ratio for 1 deg : 1 mm z in counts
```

```
$RATIO = $SLOPE*$UniR 'MaxPower/MinPower for the depths covered times
                        'the ratio needed such that A and Z moves 1:1

//////////////////FABRICATION STARTS//////////////
GEAR A OFF

G92 X0 Y0 Z0 'coordinate origin'
DWELL 1
VELOCITY ON

ABSOLUTE
LINEAR Z -$LDEPTH_INI A $DEG_INI F1
'goes down to initial depth and initial angle for writing
'PROGRAM PAUSE 'check z = -0.03050
GEAR A MASTERCONFIG Z 1 'set slave axis as A and master axis as Z position command
GEAR A RATIO $RATIO 1 'axis A moves $Ratio for every 1 count of Z
GEAR A ON

REPEAT $N_ZIGZAG
    FOR $IND1 = 1 TO $N_PORE STEP +1
        ABSOLUTE
    ShutterOpen
    DWELL 0.15
     LINEAR Z -$LDEPTH_FIN F $SPEED
     'writes up until depth_fin and with the gear on, angle should change accordingly
     ShutterClose
     'PROGRAM PAUSE 'check z=-0.00323 y A=49.20 y power = 40.7 mW o 9.25 nJ

     INCREMENTAL
     LINEAR X $PORE_SEP F $SPEED_pore 'moves to next xposition
     ABSOLUTE
LINEAR Z -$LDEPTH_INI F $SPEED 'moves back down to start always from bottom to top
    NEXT $IND1

    INCREMENTAL
    LINEAR Y -$PORE_SEP X -$PORE_SEP F $SPEED_pore 'moves to the next line

    FOR $IND2 = 1 TO $N_PORE STEP +1
     ABSOLUTE
     ShutterOpen
     DWELL 0.15
```

```
     LINEAR Z -$LDEPTH_FIN F $SPEED
'writes up until depth_fin and with the gear on, angle should change accordingly
     ShutterClose

     INCREMENTAL
    LINEAR X -$PORE_SEP F $SPEED_pore 'moves to next xposition
  ABSOLUTE
  LINEAR Z -$LDEPTH_INI F $SPEED 'moves back down to start always from bottom to top
    NEXT $IND2

    INCREMENTAL
    LINEAR Y -$PORE_SEP X + $PORE_SEP F $SPEED_pore 'moves to the next line
ENDREPEAT

GEAR A OFF
INCREMENTAL
LINEAR Y -($ARRAY_SEP-$PORE_SEP) F $SPEED_array 'moves to next array for next power
ABSOLUTE
LINEAR Z 0 A 41.15 F1 'moves to surface and lowest power to check focus

END PROGRAM
```

Bibliography

[1] I. Bernardeschi, M. Ilyas, and L. Beccai, "A review on active 3d microstructures via direct laser lithography," *Advanced Intelligent Systems*, vol. 3, no. 9, p. 2100051, 2021.

[2] J. R. Brown, A. P. Hibbins, C. R. Lawrence, M. J. Lockyear, and J. R. Sambles, "Microwave resonances of ultrathin hexagonally symmetric microcavity arrays," *Journal of Applied Physics*, vol. 112, 07 2012. 014904.

[3] G. De Pasquale, "Additive manufacturing of micro-electro-mechanical systems (mems)," *Micromachines*, vol. 12, no. 11, 2021.

[4] L. Brigo, A. Urciuolo, S. Giulitti, G. Della Giustina, M. Tromayer, R. Liska, N. Elvassore, and G. Brusatin, "3d high-resolution two-photon crosslinked hydrogel structures for biological studies," *Acta Biomaterialia*, vol. 55, pp. 373–384, 2017.

[5] R. Stoian and J. Bonse, *Ultrafast Laser Nanostructuring — The Pursuit of Extreme Scales*. Springer Nature Switzerland, 04 2023.

[6] A. Ródenas Seguí, *Subtractive 3D Laser Nanolithography of Crystals by Giant Wet-Chemical Etching Selectivity*, pp. 725–757. Cham: Springer International Publishing, 2023.

[7] G. Eaton, Shane M.; Cerullo and R. Osellame, "Illustration of the interaction physics of focused femtosecond laser pulses." Reproduced as Figure 1.2 in [8], 2012.

[8] R. Osellame, G. Cerullo, and R. Ramponi, *Femtosecond Laser Micromachining*. Springer, jan 2012.

[9] C. Roques-Carmes, N. Rivera, A. Ghorashi, S. E. Kooi, Y. Yang, Z. Lin, J. Beroz, A. Massuda, J. Sloan, N. Romeo, Y. Yu, J. D. Joannopoulos, I. Kaminer, S. G. Johnson, and M. Soljačić, "A framework for scintillation in nanophotonics," *Science*, vol. 375, no. 6583, p. eabm9293, 2022.